Progress In Electromagnetics Research, PIER 103, 101–114, 2010

POLARIZATION-TUNABLE NEGATIVE OR POSITIVE REFRACTION IN SELF-COMPLEMENTARINESS-BASED EXTRAORDINARY TRANSMISSION PRISM

M. Navarro-Cía, M. Beruete, F. Falcone, and M. Sorolla

Millimeter and Terahertz Waves Laboratory
Universidad Pública de Navarra
Campus Arrosadía, Pamplona 31006, Spain

I. Campillo

CIC nanoGUNE Consolider
Tolosa Hiribidea 76, 20018 Donostia, Spain

Abstract—Here we report a prism made of stacked quasi-self-complementary extraordinary transmission surfaces which allows simultaneously left- and right-handed propagation within the V-band for vertical and horizontal polarizations, respectively and right-handed propagation within the W-band for both polarizations. The numerical dispersion diagram of the infinite structure and effective indexes of refraction retrieved from S-parameters under normal incidence together with the finite integration time domain simulations predict single negative and double positive birefringence. The unusual type of birefringence single negative and regular double positive birefringence are afterwards demonstrated experimentally at the millimeter-waves (V- and W-bands) by the wedge experiment which lets us check, using a straightforward geometrical method, the refraction of each component. The effective index of refraction is retrieved via the Snell's law and compared to those obtained through the dispersion diagram and the retrieval method from S-parameters computed with the commercial software CST Microwave Studio^{TM}.

1. INTRODUCTION

The analysis of light transmission through holes has a long history, tracing back to the beginning of the 20th century [1] with golden years in the 1950s, 1960s and 1970s in microwave engineering [2–4]. However,

Corresponding author: M. Navarro-Cía (miguel.navarro@unavarra.es).

a new surge of interest in perforated plates, in particular subwavelength holes, followed the remarkable study of enhanced transmission through sublambda periodic hole arrays [5]. The transmission observed overcame Bethe's predictions [6] and was termed extraordinary optical transmission (EOT).

On the other hand, in the past few years left-handed media (LHM) studied theoretically by Veselago in the late 1960s [7] have evolved from perplexing to prophetic after the discovery of a non-magnetic particle with a strong magnetic response, the split ring resonator [8] and the experimental realization of those media at microwaves [9]. Among others, one major consequence of these media is negative refraction, which also leads to the remarkable property of perfect lens [10]. Now, there is an active research on finding low-loss LHM at higher frequencies where the strategies based on split ring resonators lose their good performance [11].

Recently, it has been shown that both electromagnetic phenomena, EOT and LHM, can merge in the same structure, coined as extraordinary transmission metamaterial (ETM), so as to overcome losses at millimeter-waves [12]. Notice that ETM is an optimized version of the so-called fishnet structure [13, 14] in terms of enhanced transmission phenomenon. We have confirmed the left-handed behavior by interferometric techniques [12] and wedge experiment [15, 16]. In addition, we have designed demultiplexers [17] and profiled lenses [18–20] using these concepts. Moreover, our approach has been successfully replicated at near-infrared [21] which proves the potential at any region of the spectrum of the close-stacking of subwavelength hole arrays to achieve a low-loss ETM.

A further extension of the electromagnetic properties of the simple holey pattern is achieved by the inclusion of a vertical slit connecting holes. For the single layer configuration, where Babinet's principle is applicable, the EOT structure becomes an efficient linear polarizer [22], and the multilayer configuration gives rise, after a fine-tuning, to a left-handed (to the extent that supports a backward wave, not to confuse with the handedness of the polarization state) linear polarizer [23]. Moreover, the width of the slits provides an additional degree of freedom that can be used to overlap the left-handed mode under vertical polarization E_y (incident electric field along the slits) with the right-handed mode under horizontal polarization E_x. This has been applied successfully to polarization rotation [24]. Therefore, the structure exhibits birefringence with the unconventional property that the phase constant has the opposite sign for each polarization. In order to experimentally retrieve the value of each index of refraction, we have recently embarked on the measure of a wedge configuration [25] because

the index of refraction retrieved from scattering parameters lacks the physical meaning of refraction, unless verified by Snell's law [26]. A picture of the prism can be found in Fig. 1. Its unit cell parameters are: in-plane periodicities $d_x = 2.3\,\text{mm}$, $d_y = 5\,\text{mm}$, longitudinal periodicity $d_z = 0.85\,\text{mm}$, hole size $a = 1.8\,\text{mm}$, slit width $s = 0.6\,\text{mm}$ and metal (copper) thickness $w = 0.35\,\text{mm}$. The effective zone of the wedge comprises 21 slits (and the corresponding number of lines of holes) and 11 horizontal rows, which means a $55\,\text{mm} \times 48.3\,\text{mm}$ size. Accounting for the frame assembly, the prism has total dimensions of $65\,\text{mm}/45\,\text{mm} \times 91\,\text{mm} \times 65\,\text{mm}$ (length $\times$ width $\times$ height).

In this paper, we not only restrict our analysis to the overlapping band (whose initial investigation has been already reported in [26]), but also study the second mode of each polarization (both exhibiting right-handed propagation). From this wideband characterization we are able to report two kinds of birefringence: an anomalous birefringence where one characteristic wave propagates backward and the other forward, and a regular birefringence where both characteristic waves propagate forward but with different phase velocities. We also discuss the condition for grating lobes that may disturb the experiment and give the experimental angular power distribution at three different distances covering the reactive and radiating near-field zone for co- and cross-polar measurements (the receiver antenna lined up with the transmitter or rotated 90 deg with respect to it, respectively). The experimental results are correlated with eigenmode numerical calculations and finite integration time and frequency domain simulations, performed with CST Microwave Studio^{TM}.

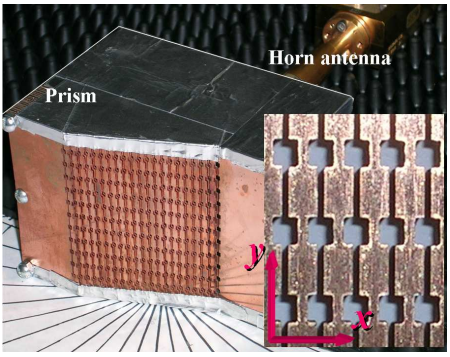

Figure 1. Picture of the prototype whose angle is 20.28 deg. The horn antenna that excites the prism can be seen on the top right of the illustration. Inset: detail of the basic perforated layer.

2. DESIGN AND NUMERICAL ANALYSIS

We first compute the dispersion diagram of the infinite structure by using the eigenmode solver of the commercial software CST Microwave Studio^{TM} and, from it, derive the effective index of refraction (see Fig. 2). For this purpose, we take the unit cell and apply periodic boundary conditions with specific phase shift across the cell along the longitudinal dimension, i.e., the stack direction, whereas in the cross-sectional dimensions electric and magnetic walls are employed. The electromagnetic wave propagating in this artificial waveguide, thus, resembles a TEM plane wave [27]. The polarization of the wave is modified to study the birefringence of the structure, and thus, the position of the electric and magnetic walls must be changed in each case. We have modeled metal as a perfect electrical conductor, since the frequencies examined here are much smaller than the bulk frequency of metals.

It is readily seen that, within the frequency range between 52 and 57.5 GHz, an overlap of the fundamental left- and right-handed propagation modes is expected. On the other hand, the second modes start from 81.5 GHz and 65.5 GHz for the vertical and horizontal polarizations respectively, and both undergo positive slope, that is, forward characteristic.

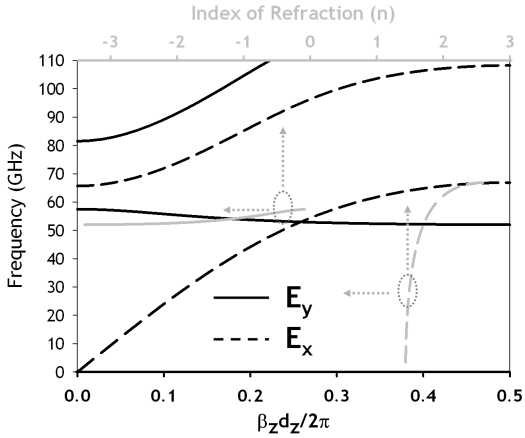

Figure 2. Dispersion diagram (black curve) and index of refraction (gray curve) for the first propagating modes calculated numerically for the infinite stack; Solid lines correspond to electric field impinging vertically (E_y), whereas dashed lines represent the response under horizontal polarization (E_x); Dotted blue arrows indicate the corresponding axes to the curve.

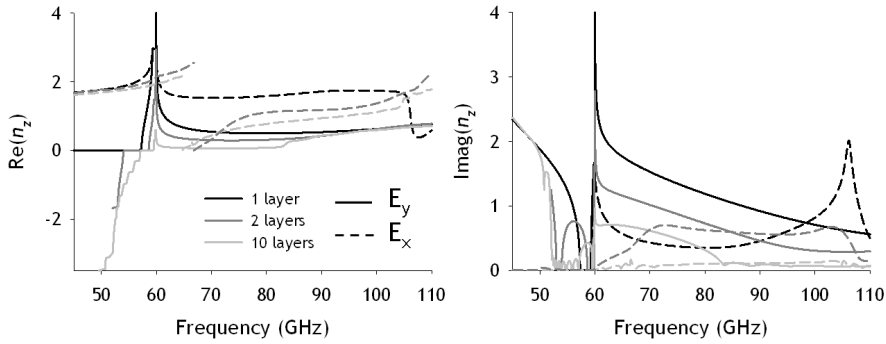

Figure 3. Real (left) and imaginary (right) parts of the effective index of refraction for 1 (black), 2 (dark gray), and 10 perforated plates (gray), when the incident electric field is E_y (solid) and E_x (dashed).

To complement the dispersion diagram, the effective indexes of refraction retrieved from S-parameters under normal incidence [28, 29] for three different numbers of stacked metasurfaces are illustrated in Fig. 3. In this case, metal has been modeled as copper with constant conductivity $\sigma = 5.8 \times 10^7$ S/m to account for metal losses, and the frequency domain solver of CST Microwave Studio^{TM} has been used with unit cell as boundary conditions. From that plot, remarkable conclusions can be derived:

(i) The horizontal axis (dashed lines) supports two positive refractive index modes (right-handed propagation) within our frequency bandwidth. The second mode may suffer more attenuation than the first one because of higher imaginary part of the index of refraction.

(ii) The vertical axis (solid lines) displays a negative refractive index mode (left-handed propagation) in the multilayer case at lower frequencies, whereas at higher frequencies the mode displays positive refractive index. Notice that the single layer configuration does not exhibit negative refractive index (assuming this effective refractive index as a mere mathematical tool since it is meaningless to assign index of refraction to a non-bulk structure). Explanation of this feature in terms of equivalent circuit model can be found in [12, 26, 27].

The next step is to build the prism. To this end, perforated plates with different numbers of vertical rows along x are stacked (one layer has one row less than its preceding layer) (see Fig. 1). Due to the finite size of the unit cell, a stepped interface is unavoidable. Therefore, in

addition to the zeroth order refracted outgoing beam, the prism, and in fact all metamaterial prisms reported up to now, behaves as a grating, which may cause diffracted beams [30]. The equation that governs gratings is,

$$n_{ETM} \times \sin(\theta_1) + \frac{m\lambda}{d} = n_2 \times \sin(\theta_2) \tag{1}$$

In this equation, we can relate the first term on the left to the refraction phenomenon (Snell's law) and the second to diffraction.

From Eq. (1) and taking $n_2 = 1$ (air), the presence of diffracted beams depends on two factors: the wavelength-grating step-ratio and the index of refraction of the prism. When $\lambda \gg d$, the equality cannot be fulfilled unless the effective index of refraction is largely negative. On the other hand, when λ approaches the spacing, diffracted beams are potentially expected when the effective index of refraction of the prism is not large. In the particular case of our design, the wavelength-grating step-ratio and effective refractive index are large and small enough respectively to prevent diffracted beams at the overlapping frequency as shown in Fig. 4. With regard to the higher band, we would record the diffracted beam $m = -1$ within the range 100 to 110 GHz, if our experimental setup allowed us to scan up to -90 deg. However, our limit is -60 deg, and thus, we do not expect to scan any diffracted beam in the second band of any polarization.

To finish with the numerical analysis, we run some finite integration time domain simulation to check the behavior of the prism. To reduce computation effort, a 2D geometry has been considered because it can give most of the information on the transmission

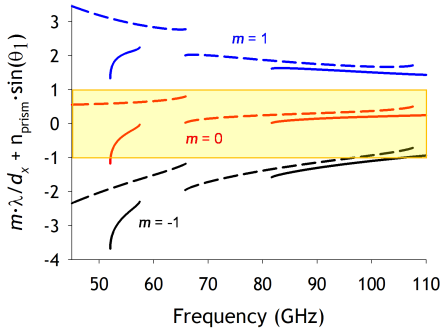

Figure 4. Conditions for the generation of zeroth and first ($m = \pm 1$) higher order diffracted beams. (solid curves) Ey; (dashed curves) Ex. The zone where $\sin(\theta_2)$ has meaning is the yellow-filled one, and it demonstrates the absence of diffracted beams in our prototype.

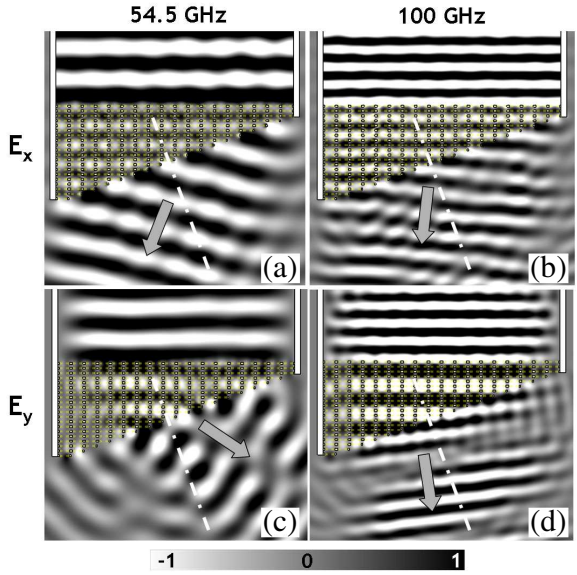

Figure 5. Electric field evolution at $f = 54.5\,\text{GHz}$ (left) and 100 GHz (right) for horizontal E_x (top) and vertical polarization E_y (bottom). The normal and the angle of deflection have been highlighted to guide the eye.

characteristics of the addressed wedge experiment. The incident beam is launched from the top of the computational domain, and the prism is placed in the lower region. The aperture is formed by the defined waveguide and with the wedge sample placed directly at the end of it. The channel extended from where the incident wave is launched up to the first interface of the wedge has a length of 15 mm. The results can be found in Fig. 5. Notice that the beam undergoes negative refraction only in plot (c), which corresponds to the vertical polarization E_y and the frequency at which we expect left-handed propagation. The other cases linked, respectively, with the second mode of this polarization (plot (d)), and the horizontal polarization modes (plot (a) and (b)) display undoubtedly positive refraction.

3. EXPERIMENTAL SETUP AND RESULTS

The description of the experimental setup is as follows. The prism is illuminated from the back by a corrugated horn antenna (needless to say, in order to cover the whole bandwidth, two antennas have

been used: one for the V-band and the other for the W-band), and the outgoing beam deflection is scanned at three different distances $z = 100\,\text{mm}$, 400 mm and 600 mm by another identical corrugated horn antenna. Both antennas are connected to the AB-Millimetre^{TM} quasi-optical vector network analyzer. The frequency band and effective aperture used impose that we are dealing with near field or Fresnel zone due to the fact that $2D^2/\lambda \approx 1100\,\text{mm}$, where D is the largest dimension of the prism [31]. Besides, for the receiver distance of 100 mm, we are in the limit between the reactive near-field distance and radiating near-field, since $0.62(D^3/\lambda)^{0.5} \approx 100\,\text{mm}$ [31]. The calibration or reference is done by using a face to face antennas configuration for each distance.

The experimental spatial power distribution along the xz-plane as a function of the frequency is mapped in Fig. 6 for each distance for co-polar measurements. The maps of spatial field distribution as shown

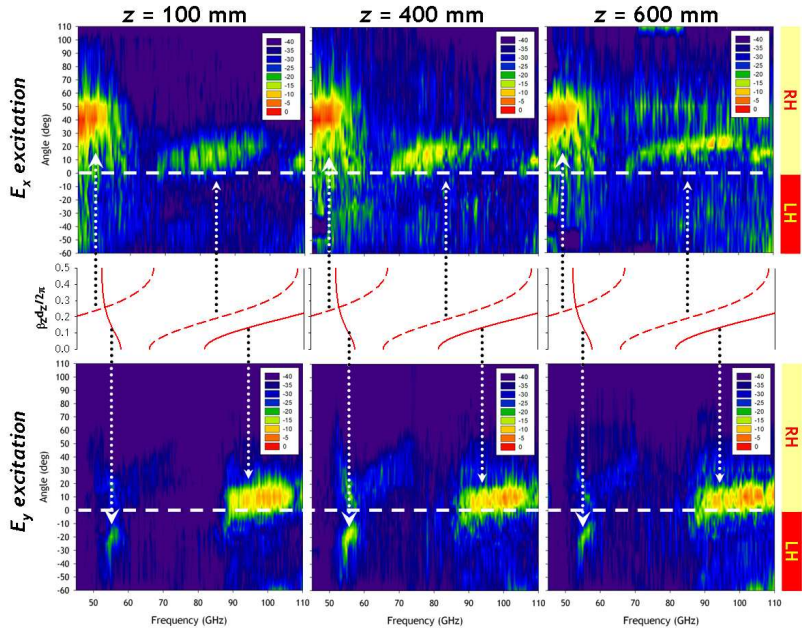

Figure 6. Top and bottom) Spatial power distribution in logarithm scale along xz-plane for receiving distances of $z = 100\,\text{mm}$, 400 mm, and 600 mm respectively starting from the left under: horizontal illumination (top) vertical illumination (bottom). (Middle) Numerical dispersion diagram plotted for comparison purpose with experimental results. Arrows have been used to correlate propagating bands of dispersion diagram and experimental results. Color scale from 0 to $-40\,\text{dB}$ in steps of 5 dB.

from the left to the right are at $z = 100\,\text{mm}$, $400\,\text{mm}$, and $600\,\text{mm}$ respectively, and all angles are relative to the surface normal.

The pattern of warm color spots in the top plots of Fig. 6 reveals two enhancement transmission zones:

(i) One is in the lower part of our experimental bandwidth, which corresponds to the horizontal first propagating mode. This mode arises as a result of the parallel plate waveguide defined by the slit array under electric field perpendicular to the metal faces, that is, horizontal illumination in our terminology. The positive refraction of this mode is clear.

(ii) The other is in the central and upper region of the measurement and is the second horizontal propagating mode. This mode displays specially a gap around 100 and 105 GHz in the two closer distances to the prism ($z = 100$ and $400\,\text{mm}$), and its origin may be found in the finiteness of the structure or in the fact of dealing with near-field tests. Again, there are no doubts of the right-handedness response of the mode. Also notice that, as it is expected from the retrieved effective refractive index (Fig. 3), the transmittance is lower for this mode than for the first propagating mode.

On the other hand, the spots in the bottom plots of Fig. 6 bring to light also two enhanced transmission zones, but with rather different characteristics:

(i) One region is between 50 and 60 GHz and undergoes a noticeable negative refraction. This is the LH mode related to the ET stack [12, 15, 16].

(ii) The second propagating mode of the vertical polarization starts approximately at 90 GHz and is positively refracted accounting then for right-handed propagation.

All these propagation features correlate in general well with the numerical dispersion diagram, which has been represented together with the experimental results in-between of them, although we are working in near field zone and with a finite structure. In fact, notice that $z = 600\,\text{mm}$ agrees better with the dispersion diagram than the other two distances, as it is expected since it is closer to the far-field limit. Besides, to guide the eye, arrows have been drawn to highlight the match of numerical eigenmodes with experimental propagating bands. Nevertheless, by giving a closer look between dispersion diagram and experimental results, some undesirable details come into view. The most important one is that the first propagating mode of the horizontal polarization diminishes abruptly from 55 GHz rather than extending up to 65 GHz. Therefore, the expected overlap between

this horizontal right-handed mode and the vertical left-handed band expected for this particular design is not completely fulfilled. Anyway, the proof of the operation of this birefringent prism is undoubtedly demonstrated.

Moving from the qualitative description of the previous paragraph, a quantitative comparison between numerical and experimental results in terms of effective index of refraction can be seen in Fig. 7. There, the effective index of refraction derived from the experimental results via Snell's law for both polarizations alongside the experimental error bars are plotted, and the index computed through the dispersion diagram is also shown superimposed. The good agreement between numerical and experimental results is remarkable despite the fact already pointed out regarding near-field measurement and the edge effects arisen from the finiteness of the structure.

To finish with the characterization of the propagating properties of the proposed prism, the cross-polar experimental results (receiving antenna orthogonal to the transmitting antenna) were also recorded (see Fig. 8). While the cross-polar measurement of the vertical polarization does not display anything worth mentioning apart from attractive low cross-polarization, the cross-polar of the horizontal polarization shows some relative high values between 60 and 70 GHz at around 30 deg. If one has a closer look to Fig. 6 at those frequencies, a slightly enhancement of the transmittance is observed along the same positive angles for the vertical polarization E_y. Thus, this may be the manifestation of an evanescent wave generated by the corrugated interface and the finiteness of the aperture [32].

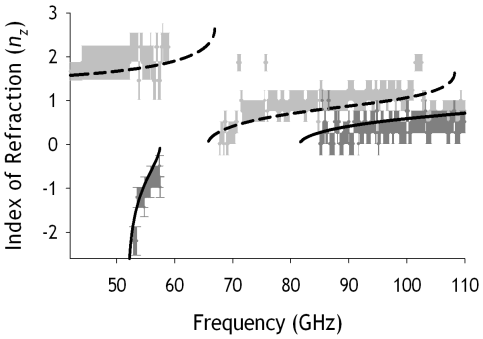

Figure 7. Evolution of the effective refractive index as a function of the frequency for both polarizations. Gray (E_x) and dark gray spots (E_y) are the experimental points along with the corresponding error bars. Black curves are the equivalent simulation results derived from the dispersion diagram: E_x (dashed lines) and E_y (solid lines).

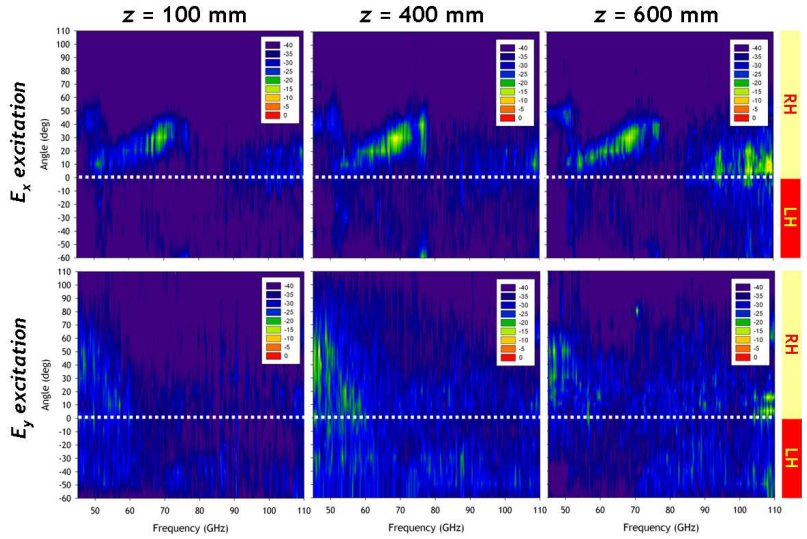

Figure 8. (Top and bottom) Cross-polarization spatial power distribution along xz-plane for receiving distances of $z = 100\,\text{mm}$, 400 mm, and 600 mm respectively starting from the left under: horizontal illumination (top) vertical illumination (bottom). Color scale from 0 to $-40\,\text{dB}$ in steps of 5 dB.

4. CONCLUSIONS

An in-depth analysis of a free-standing single negative and double positive birefringence metamaterial has been performed at millimeter-waves both numerically and experimentally. It has been shown that the single negative birefringence happens within the cut-off regime of the holes (at the EOT regime), whereas the regular double positive birefringence takes place when the apertures are above cut-off. Several types of numerical calculations have been carried out to investigate the behavior of the stacked structure for the two first propagating modes of each polarization: eigenmode computations for the dispersion diagram, finite integration time domain simulation for the beam deflection visualization in the wedge experiment and finite integration frequency domain simulations to retrieve the effective index of refraction from S-parameters. In addition, a discussion of grating lobes has been given to arrive at the conclusion that they are not expected for the prism presented here. Finally, the prism has been tested within the Fresnel zone at three different distances under co- and cross-polar measurements. The experimental results obtained agree well with the

numerical ones. This approach extends the concept of birefringence and can find application in the design of frequency and polarization (de)multiplexing devices at any frequency of the spectrum.

ACKNOWLEDGMENT

This work has been supported by the Spanish Government under contracts Consolider "Engineering Metamaterials" CSD2008-00066 and TEC2008-06871-C02-01.

REFERENCES

1. Garcia de Abajo, F. J., "Colloquium: Light scattering by particle and hole arrays," *Rev. Modern Phys.*, Vol. 79, No. 4, 1267–1290, 2007.
2. Brown, J., "Artificial dielectric having refractive indices less than unity," *Proc. IEE*, Vol. 100, No. 4, 51–62, 1953.
3. Ulrich, R., "Far-infrared properties of metallic mesh and its complementary structure," *Infrared Phys.*, Vol. 7, No. 1, 37–55, 1967.
4. Chen, C. C., "Diffraction of electromagnetic waves by a conducting screen perforated periodically with circular holes," *IEEE Trans. Microwave Theory Tech.*, Vol. 19, No. 5, 475–481, 1971.
5. Ebbesen, T. W., H. J. Lezec, H. Ghaemi, T. Thio, and P. A. Wolf, "Extraordinary optical transmission through sub-wavelength hole arrays," *Nature*, Vol. 391, No. 6668, 667–669, 1998.
6. Bethe, H. A., "Theory of diffraction by small holes," *Phys. Rev.*, Vol. 66, No. 7–8, 163–182, 1944.
7. Veselago, V. G., "The electrodynamics of substances with simultaneously negative values of ε and μ," *Soviet Phys. Ups.*, Vol. 10, No. 4, 509–514, 1968.
8. Pendry, J. B., A. J. Holden, D. J. Robbins, and W. J. Stewart, "Magnetism from conductors and enhanced nonlinear phenomena," *IEEE Trans. Microw. Theory Tech.*, Vol. 47, No. 11, 2075–2084, 1999.
9. Smith, D. R., W. J. Padilla, D. C. Vier, S. C. Nemat-Nasser, and S. Schultz, "Composite medium with simultaneously negative permeability and permittivity," *Phys. Rev. Lett.*, Vol. 84, No. 18, 4184–4187, 2000.

10. Pendry, J. B., "Negative refraction makes a perfect lens," *Phys. Rev. Lett.*, Vol. 85, No. 18, 3966–3969, 2000.
11. Solymar, L. and E. Shamonina, *Waves in Metamaterials*, Oxford University Press, New York, 2009.
12. Beruete, M., M. Sorolla, and I. Campillo, "Left-handed extraordinary optical transmission through a photonic crystal of subwavelength hole arrays," *Opt. Express*, Vol. 14, No. 12, 5445–5455, 2006.
13. Zhang, S., W. Fan, N. C. Panoiu, K. J. Malloy, R. M. Osgood, and S. R. J. Brueck, "Experimental demonstration of near-infrared negative-index metamaterials," *Phys. Rev. Lett.*, Vol. 95, No. 13, 137404-1-4, 2005.
14. Dolling, G., C. Enkrich, M. Wegener, C. M. Soukoulis, and S. Linden, "Simultaneous negative phase and group velocity of light in a metamaterial," *Science*, Vol. 32, No. 5775, 892–894, 2006.
15. Navarro-Cía, M., M. Beruete, M. Sorolla, and I. Campillo, "Negative refraction in a prism made of stacked subwavelength hole arrays," *Opt. Express*, Vol. 16, No. 2, 560–566, 2008.
16. Beruete, M., M. Navarro-Cía, F. Falcone, I. Campillo, and M. Sorolla, "Connection between extraordinary transmission and negative refraction in a prism of stacked subwavelength hole arrays," *J. Phys. D: Appl. Phys.*, Vol. 42, No. 16, 165504-1-4, 2009.
17. Navarro-Cía, M., M. Beruete, I. Campillo, and M. Sorolla, "Millimeter-wave left-handed extraordinary transmission metamaterial demultiplexer," *IEEE Antennas Wireless Propag. Lett.*, Vol. 8, No. 1, 212–215, 2009.
18. Beruete, M., M. Navarro-Cía, M. Sorolla, and I. Campillo, "Planoconcave lens by negative refraction of stacked subwavelength hole arrays," *Opt. Express*, Vol. 16, No. 13, 9677–9683, 2008.
19. Navarro-Cía, M., M. Beruete, M. Sorolla, and I. Campillo, "Converging biconcave metallic lens by double-negative extraordinary transmission metamaterial," *Appl. Phys. Lett.*, Vol. 94, No. 14, 144107-1-3, 2009.
20. Navarro-Cía, M., M. Beruete, M. Sorolla, and I. Campillo, "Viability of focusing effect by left-handed stacked subwavelength hole arrays," *Phys. B*, 2010 (in press).
21. Valentine, J., S. Zhang, T. Zentgraf, E. Ulin-Avila, D. A. Genov, G. Bartal, and X. Zhang, "Three-dimensional optical metamate-

rial with a negative refractive index," *Nature*, Vol. 455, No. 7211, 376–379, 2008.

22. Beruete, M., M. Navarro-Cía, I. Campillo, P. Goy, and M. Sorolla, "Quasioptical polarizer based on self-complementary sub-wavelength hole arrays," *IEEE Microw. Wirel. Comp. Lett.*, Vol. 17, No. 12, 834–836, 2007.
23. Beruete, M., M. Navarro-Cía, M. Sorolla, and I. Campillo, "Polarized left-handed extraordinary optical transmission of subterahertz waves," *Opt. Express*, Vol. 15, No. 13, 8125–8134, 2007.
24. Beruete, M., M. Navarro-Cía, M. Sorolla, and I. Campillo, "Polarization selection with stacked hole array metamaterial," *J. Appl. Phys.*, Vol. 103, No. 5, 053102-1-4, 2008.
25. Shelby, R. A., D. R. Smith, and S. Schultz, "Experimental verification of a negative index of refraction," *Science*, Vol. 292, No. 5514, 77–79, 2001.
26. Beruete, M., M. Navarro-Cía, F. Falcone, I. Campillo, and M. Sorolla, "Single negative birefringence in stacked spoof plasmon metasurfaces by prism experiment," *Opt. Lett.*, Vol. 35, No. 5, 643–645, 2010.
27. Beruete, M., I. Campillo, M. Navarro-Cía, F. Falcone, and M. Sorolla Ayza, "Molding left- or right-handed metamaterials by stacked cutoff metallic hole arrays," *IEEE Trans. Antennas Propag.*, Vol. 55, No. 6, 1514–1521, 2007.
28. Chen, X., T. M. Grzegorczyk, B.-I. Wu, J. Pacheco, Jr., and J. A. Kong, "Robust method to retrieve the constitutive effective parameters of metamaterials," *Phys. Rev. E*, Vol. 70, No. 1, 016608-1-7, 2004.
29. Hao, Y. and R. Mittra, *FDTD Modeling of Metamaterials: Theory and Applications*, Artech House, Norwood, 2009.
30. Smith, D. R., P. M. Rye, J. J. Mock, D. C. Vier, and A. F. Starr, "Enhanced diffraction from a grating on the surface of a negative index material," *Phys. Rev. Lett.*, Vol. 93, No. 13, 137405-1-4, 2004.
31. Balanis, C. A., *Antenna Theory Analysis and Design*, John Wiley and Sons, New York, 1997.
32. Depine, R. A. and A. Lakhtakia, "Plane-wave diffraction at the periodically corrugated boundary of vacuum and a negative-phase-velocity material," *Phys. Rev. E*, Vol. 69, No. 5, 057602-1-4, 2004.